Photovoltaic-Active Dithienosilole-Containing Polymers

Liang Liao and Liming Dai*

Department of Chemical and Materials Engineering, University of Dayton, 300 College Park, Dayton, Ohio 45469-0240

Adam Smith and Michael Durstock*

Materials and Manufacturing Directorate, Air Force Research Laboratory, Wright-Paterson AFB, Ohio 45433

Jianping Lu,* Jianfu Ding, and Ye Tao

National Research Council of Canada, 1200 Montreal Road, Ottawa, Canada, K1A 0R6

Received August 13, 2007; Revised Manuscript Received October 17, 2007

ABSTRACT: Silole-containing polymers consisting of a dithienosilole homopolymer backbone (**12**) or an alternating dithienosilole and 4,7-bis(2-thienyl)-2,1,3-benzothiadiazole copolymer backbone (**13**) were synthesized. The presence of planar dithienosilole tricyclic units along these π-conjugated polymer backbones lowered the band gap and led to strong absorption in the visible region of the solar spectrum. The introduction of electron-withdrawing benzothiadiazole moieties along the dithienosilole backbone further reduced the optical band gap and increased the interchain interaction. Bulk-heterojunction organic solar cells using 1:1 w/w polymer **12** or **13**:PCBM (methanofullerene [6,6]-phenyl C61-butyric acid methyl ester) blends as the photoactive layers were prepared. Photovoltaic cells with copolymer **13** as the electron donor and PCBM as the electron acceptor exhibited an increased energy conversion efficiency by a factor of 3 up to 0.18% under an AM 1.5 simulated solar light at 100 mW/cm^2 after thermal annealing at 140 °C.

Introduction

Owing to its strong electron affinity, high fluorescent efficiency,[1,2] photostability, and chemical stability,[3] the silole (silacyclopentadiene) ring (**1** in Scheme 1) and its derivatives have attracted much attention as functional building units for the development of advanced organic materials. In fact, silole has the lowest LUMO energy level as well as a relatively high-lying HOMO level among many heteroarene monomer units of π-conjugated polymers, such as pyrrole, furan, thiophene, and pyridine. As a consequence, poly(2,5-silole) has the lowest band gap.[4] Therefore, π-conjugated polymers containing silole rings with a low-lying LUMO level and an enhanced carrier mobility have recently been used as novel optoelectronic materials for applications in electroluminescent devices[4−9] and organic thin-film transistors.[10,11] Since low energy-gap materials (∼1.5 eV) could match well to the solar spectrum,[12] silole-containing conjugated polymers should also be useful for applications in organic solar cells.

We report here the synthesis of solution-processable π-conjugated polymers containing dithienosilole (DST) moieties along their backbones *via* a Stille reaction between dithienosilole distannane and aryl dibromides for potential applications in organic solar cells. The incorporation of a silicon bridge into a bithienyl moiety (e.g., **2a** in Scheme 1) significantly reduces the HOMO−LUMO gap of **2a** due to the newly formed extended planar π-conjugated tricyclic system[7,13,14](dithienosilole in Scheme 1) and $\sigma^*-\pi^*$ conjugation between the σ^*-orbit of silicon and π^*-orbit of the bithiophene unit.[6,8,11] The alkyl substitutions at the silicon of DTS units are necessary in order to produce soluble π-conjugated polymers containing sufficiently long dithienosilole segments for potential applications in optoelectronic polymer devices. In particular, we prepared dithienosilole-containing homopolymer **12** and a conjugated copolymer **13** comprising alternating dithienosilole and 4,7-dithieyl-2,1,3-benzothiadiazole in this study, as shown in Scheme 2. Compared with homopolymer **12**, the synthesis of the fully conjugated aromatic copolymer **13** with strong internal electron donor−acceptor interactions could further narrow the band gap.[15−17] As expected, polymer **13** exhibited a much broader strong absorption over the solar spectrum than polymer **12**. It was further found that the absorption maximum of polymer **13** in solution red-shifted by about 30 nm upon the formation into a thin film. This observation is an indication for the presence of strong interchain interactions in the solid state through 2D $\pi-\pi$ stacking, which can enhance charge carrier mobilities favorable for applications in various optoelectronic devices including organic solar cells.[18,19] In contrast, there was no observable shift in the absorption peak of polymer **12** from solution to the solid-state film, implying a weak interchain interaction in the polymer **12** film.

Scheme 1

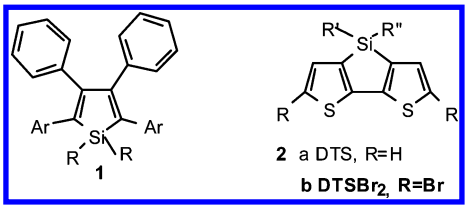

In order to translate the above structure-specific properties into optoelectronic devices with unique characteristics, we prepared bulk-heterojunction organic solar cells using 1:1 wt/wt polymer **12** or **13**:PCBM blends as the photoactive layers. Because of its more extended conjugation and the associated

* Corresponding authors. E-mail: (L.D.) ldai@udayton.edu; (M.D.) Michael.durstock@wpafb.af.mil; (J.L.) Jianping.Lu@nrc-cnrc.gc.ca.

10.1021/ma071825x CCC: $37.00
Published on Web 11/28/2007

Scheme 2. Syntheses and Structures of Polymers 12 and 13

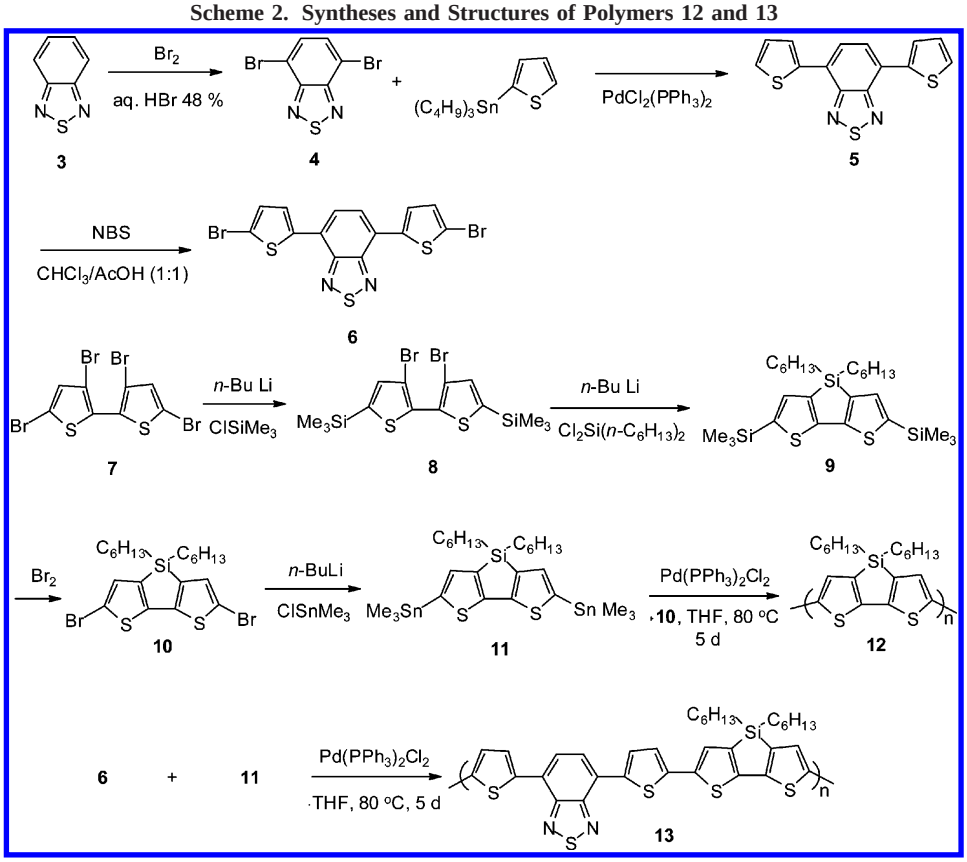

stronger absorption over the solar spectrum, polymer **13** showed superior photovoltaic performance with respect to polymer **12**. The device performance for both polymer **12** and **13** based solar cells was improved by thermal annealing. So far, the best device performance with a power conversion efficiency of 0.18% was achieved from polymer **13** based devices after thermal annealing at 140 °C. Although this value of the power conversion efficiency for these unoptimized solar cells is not sufficiently high yet, this study provides new concepts for enhancing light harvesting *via* the synthesis of silole-containing low-band gap conjugated polymers with strong internal electron donor−acceptor interactions and for improving the device performance through the morphology control of the silole-containing conjugated polymer photovoltaic layers by thermal annealing.

Experimental Section

Materials and Characterization. All reagents and solvents were purchased from Aldrich and Fisher. Anhydrous tetrahydrofuran was distilled over sodium/benzophenone under Ar prior to use. 4,7-Bis(5-bromo-2-thienyl)-2,1,3-benzothiadiazole (**6**) was synthesized from commercially available 2,1,3-benzothiadiazole via a three-step reaction sequence according to a reported procedure with some modifications.[20,21] 3,3′,5,5′-Tetrabromo-2,2′-bithiophene (**7**) was prepared by the direct bromination of 2,2′-bithiophene in $CHCl_3$/AcOH with Br_2 at 0 °C.

NMR spectra were recorded on a Bruker Avance 300 spectrometer using tetramethylsilane or trace chloroform in deuterium chloroform as internal references. Gel permeation chromatography (GPC, Viscotek TDA 302) was used for measuring the molecular weight and polydispersity index. UV−vis spectra were measured using a Perkin-Elmer Lambda 900 UV−vis−NIR spectrometer. Fluorescence spectra were recorded on a Perkin-Elmer LS 55 Luminescence spectrometer. FT-IR spectra were collected from a Perkin-Elmer Spectrum One FT-IR spectrometer. Thermogravimetric analysis (TGA) was carried out using TA Instruments TGA Q500 in air, while differential scanning calorimetry (DSC) analysis was made on a TA Instruments DSC 2920 under nitrogen.

Monomer and Polymer Syntheses. Typical Procedure for a Facile One-Pot Three-Step Synthesis of 5,5′-Dibromo-3,3′-dihexylsilylene-2,2′-bithiophene (10). To a solution of 3,3′,5,5′-tetrabromo-2,2′-bithiophene (4.82 g, 10 mmol) in THF (anhydrous, 70 mL, THF was freshly distilled over calcium hydride prior to use) was added *n*-butyllithium (10 M solution in hexane, 2.1 mL, 21 mmol) under argon atmosphere over 15 min at −95 to −98 °C and stirred for 10 min. Chlorotrimethylsilane (2281 mg, 2.68 mL, 21 mmol) was then added over 15 min. After having been stirred at −94 to −98 °C for 20−30 min, the reaction mixture was warmed to ambient temperature slowly and further stirred at ambient temperature for 3 h. TLC indicated the complete conversion of starting material.

Thereafter, the above mixture was cooled at −78 °C and *n*-butyllithium (10 M solution in hexane, 2.1 mL, 21 mmol, 2.1 equiv) was introduced over 15 min and stirred at this temperature for 10−20 min. The mixture was then warmed up to −2 to −5 °C for 18−30 min, and the mixture was cooled again to −78 °C. Dichlorodihexylsilane (2.83 g, 2.94 mL, 10.5 mmol, 1.05 equiv) was added dropwise over 20 min and then stirred at this temperature for 50 min. TLC indicated the completion of conversion.

To above mixture was added bromine (3.36 g, 1.08 mL, 21 mmol) dropwise at −78 °C and the mixture was stirred at this temperature for 50 min. The mixture was then kept at −10 to −15 °C overnight. The usual workup of reaction mixture followed by purification using silica gel column chromatography provided the analytical pure product **10** as a pale yellow oil. ^{1}H NMR ($CDCl_3$, 300 MHz) δ: 0.87 (m, 10H), 1.27 (m,16H), 7.00 (s, 2H). ^{13}C NMR ($CDCl_3$, 75.45 MHz) δ: 11.85, 14.29, 22.76, 24.20, 31.59, 33.02, 111.62, 132.36, 141.20, 149.12.

Synthesis of 5,5′-bis(trimethylstannyl)-3,3′-dihexylsilylene-2,2′-bithiophene (11). In a 100 mL flask was placed **10** (1.562 g, 3 mmol) in anhydrous THF (20 mL), to which an *n*-butyllithium−hexane solution (10 M, 0.63 mL, 6.3 mmol) was added at −78 °C under stirring for 1 h. Thereafter, the mixture solution was warmed up slowly to room temperature in an ambient environment with stirring. After the reaction mixture was cooled down to −78 °C again, a predetermined amount of trimethyltin chloride (1 M in

hexane, 6.45 mL, 6.45 mmol) was added slowly. The mixture solution was then stirred at ambient temperature for 18 h, followed by the addition of ice−water (50 g). Finally, the aqueous layer was extracted with ether (3 × 30 mL) while the combined organic layer was dried with anhydrous sodium sulfate and concentrated under a reduced pressure to give product **11** (1.77 g, 86%). ^{1}H NMR ($CDCl_3$) δ: 0.39 (s, 18H, $SnMe_3$), 0.88 (m, 10H), 1.28 (m, 16 H), 7.10 (s, 2H). ^{13}C NMR ($CDCl_3$) δ: −7.88, 12.20, 14.34, 22.83, 24.47, 31.65, 33.13, 125.03, 137.86, 143.30, 155.20. Anal. Calcd for $C_{26}H_{46}S_2SiSn_2$ (%): C, 45.37; H, 6.74; S 9.32. Found (%): C, 45.46; H, 6.53; S, 9.46.

Synthesis of Polymer 12. Into a degassed suspension of bis(triphenylphosphine)palladium(II) chloride ($Pd(PPh_3)_2Cl_2$, 7 mg, 0.01 mmol) in anhydrous THF (2.5 mL) was dropwise added a degassed solution of **10** (104 mg, 0.2 mmol) and **11** (138 mg, 0.2 mmol) in anhydrous THF (5 mL). Thereafter, the reaction mixture was stirred at ambient temperature for 5 min and then heated under reflux for 5 days. 2-(Tributylstannyl)thiophene (10 mg) and 2-bromothiophene (5 mg) were added consecutively under 1 day refluxing each to end-cap the bromo groups and trimethylstannyl groups, respectively. After the solution was cooled down to room temperature, water (10 mL) was added. The aqueous layer was then extracted by dichloromethylene (10 mL × 2) while the combined organic layer was washed with water (15 mL) and dried over anhydrous magnesium sulfate and distilled to remove the solvents. The residue was dissolved in a minimum amount of THF and was added to methanol (80 mL) under stirring. Dark purple solid was precipitated and collected by filtration. The resultant polymer sample was purified one more time by precipitation from THF/MeOH (122 mg, yield 85%). GPC: M_w 65 200; PDI 8.0. ^{1}H NMR ($CDCl_3$) δ: 0.86 (s, br, 10H), 1.26 (s, br, 16H), 7.12 (s, br, 2H). IR (film on NaCl) (cm^{-1}): 2955 (m), 2922 (s), 2871 (m), 2854 (m), 1613 (w), 1466 (m), 1353 (w), 1250 (w), 1169 (m), 1099 (w), 998 (w), 958 (w), 838 (w), 692 (w). Anal. Calcd for $C_{20}H_{28}S_2Si$ (%): C, 66.61; H, 7.83; S, 17.78. Found (%): C, 65.61; H, 7.75; S, 17.61.

Synthesis of Polymer 13. To a degassed suspension of bis(triphenylphosphine)palladium(II) chloride ($Pd(PPh_3)_2Cl_2$, 19.5 mg, 0.01 mmol) in anhydrous THF (3.5 mL) was dropwise added a degassed solution of **6** (137.5 mg, 0.3 mmol) and **11** (216.8 mg, 0.315 mmol, 1.05 equiv) in anhydrous THF (25 mL). Thereafter, the mixture solution was stirred at ambient temperature for 5 min and then heated at 78−80 °C in an oil bath for 5 days. 2-Bromothiophene (5 mg) was then added to end-cap the trimethylstannyl groups. After the solution was cooled down to room temperature, 10 mL of water was added. The aqueous layer was then extracted by dichloromethylene (10 mL × 2) while the combined organic layer was washed by water (15 mL) and dried with anhydrous magnesium sulfate to remove the solvents. The residue was dissolved in a minimum amount of THF, flitered and then added to methanol (80 mL) under stirring. Black solid was precipitated and collected by suction. The resultant polymer was purified one more time by precipitation from THF/MeOH. GPC: M_w 29 200; PDI 5.2. ^{1}H NMR ($CDCl_3$) δ: 0.89 (s, br, 10H), 1.27 (s, br, 16H), 6.91−8.10 (m, ArH, 8H). Anal. Calcd for $C_{34}H_{34}N_2S_5Si$ (%): C, 61.96; H, 5.20; N, 4.25; S, 24.32. Found (%): C, 60.51; H, 5.46; N, 4.32; S, 24.05.

Photovoltaic Device Fabrication and Characterization. Glass slides patterned with ITO (Colorado Concept Coatings LLC) were cleaned by sonicating sequentially in detergent, water, 1,1,1-trichloroethane, acetone, and methanol, followed by treatment in a low power air plasma for 15 min with a Harrick PDC-32G plasma sterilizer. Thereafter, the ITO-coated slides were spin-coated (500 rpm for 5 s, then 4000 rpm for 60 s) with a filtered (0.45 μm NYL w/ GMF syringe filter) aqueous solution of poly(ethylene dioxythiophene) doped with polystyrene sulfonic acid, PEDOT:PSS (trade name Baytron P VP AI 4083, H.C. Starck) and then transferred to a drybox. The resulting thin PEDOT:PSS layer (~35 nm) was dried in an oven under a mild N_2 purge at 120 °C for 1 h. A 1:1 (by weight) chlorobenzene solution of polymer and PCBM (10.0 mg/mL each) was stirred at 50 °C for 16 h and then spun-cast on the PEDOT−PSS-coated slides at various speeds (600−2000 rpm) for 90 s. The Al top electrode (~100 nm) was then deposited by thermal evaporation through a shadow mask, resulting in the formation of 10 distinct cells each with an active area of 0.165 cm^2. Film thicknesses were measured with a Tencor P-10 surface profiler at a stylus force of 0.6 mg. Preliminary testing of each of the ten pixels was performed to select the most promising pixel prior to full solar simulated analysis. The best performing pixel then underwent V_{oc}, I_{sc}, and dark and illuminated $I-V$ studies using an Oriel 300 W solar simulator with appropriate filters to provide AM 1.5 G (100 mW/cm^2). The fill-factor (*FF*) was determined from the illuminated $I-V$ and is the maximum power delivered divided by the product of V_{oc} and I_{sc}. For thermal annealing, devices were heated on a 0.64 cm thick aluminum plate with temperature controller in thermal contact powered by a DC supply. After first testing the devices at room temperature, tests were run at 30 °C and at 10 °C increments. External quantum efficiency (EQE) studies were performed using a tungsten source on an Acton Spectra Pro 275 monochromator with order sorting filters. The probe beam was chopped at 21 Hz and the signal detected with an EG&G PAR 5210 lock-in amplifier.

Results and Discussion

Synthesis. Dithienosilole (DTS) as a novel π-conjugated building block, in which the β,β'-positions of 2,2′-bithiophene are intramolecularly linked by a silylene bridge, has been synthesized for the development of efficient hole transporting materials for potential applications in organic light-emitting diodes[13,22] and thin film transistors.[10] Aiming at the photovoltaic application, we report in this paper an innovative one-pot procedure for the facile synthesis of dithienosilole derivatives in a good yield. Briefly, 3,3′,5,5′-tetrabromo-2,2′-bithiophene (**7**) was first selectively lithiated at the α positions and then protected with trimethylsilyl groups. The resulting compound **8** was treated with 2.0 equiv *n*-BuLi in THF at −78 °C and cyclized with dichlorodihexylsilane to produce compound **9**. Finally, the trimethylsilyl groups were cleaved with bromine at −78 °C to give the target compound 5,5′-dibromo-3,3′-dihexylsilylene-2,2′-bithiophene **10**. Compound **10** was then further selectively lithiated at the α positions and protected with trimethyltin groups to produce compound **11**. Both polymers **12** and **13** were synthesized by Stille coupling between 5,5′-bis(trimethylstannyl)-3,3′-dihexylsilylene-2,2′-bithiophene (**11**) and appropriate dibromo compounds (Scheme 2) in refluxing anhydrous THF after 5 days stirring. Since the palladium catalyst is quite sensitive to oxygen and light, the polymerization reaction was run in the dark using a standard Schlenk technique. Polymer **12** is soluble in a wide range of common organic solvents, including chloroform, tetrahydrofuran, and dichloromethane. However, the high molecular fraction of polymer **13** is not soluble in THF or chloroform because of the strong interchain aggregation induced by the rigid electron-withdrawing unit of 4,7-dithieyl-2,1,3-benzothiadiazole. Recently, Leclerc and coworkers observed a similar phenomenon on poly[*N*-9′-heptadecanyl-2,7-carbazole-*alt*-5,5-(4′,7′-di-2-thienyl-2′,1′,3′-benzothiadiazole)].[23] The weight-averaged molecular weight (M_w) and the polydispersity index (PDI) were measured by GPC using THF as an eluent and polystyrene as the standard to be 65 200 and 8.0 for polymer **12**, and 29 200 and 5.2 for the THF-soluble fraction of copolymer **13**, respectively.

Thermal Properties of Polymers 12 and 13. The thermogravimetric analysis (TGA) showed that polymers **12** and **13** are thermally stable with only about 5% weight loss in air at temperatures of 360 and 324 °C, respectively. The negligible weight loss below 300 °C can be ascribed to the high thermal stability characteristic of silole rings. DSC analysis revealed that both polymers **12** and **13** are amorphous materials with a

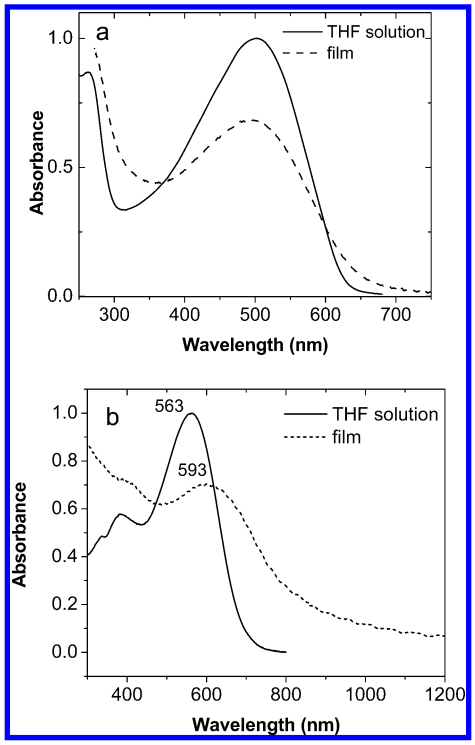

Figure 1. UV−vis spectra of polymer **12** (a) and **13** (b) in THF solutions and in the solid state.

glass transition temperature at 83 and 114 °C, respectively. The lack of crystallinity in these two polymers with the relatively high polydispersity indices (vide supra) could serve as a drawback for potential applications in organic solar cells since the formation of phase-separated ordered nanostructures in the photoactive layer is desirable for charge separation and transport.[24,25] Further optimization of the synthetic conditions could lead to low-polydispersity polymers with a high crystallinity.

Optoelectronic Properties. UV—Vis Absorptions. Figure 1 shows the UV−vis spectra for polymers **12** and **13**, in both a solution (THF) and the solid state, respectively. As can be seen in Figure 1a, broad absorption bands well located in the visible region were observed for both the solution and film of **12**. The maximum absorbance wavelength (502 nm) for **12** in THF is about 144 nm red-shifted from the corresponding absorption wavelength (348 nm) of its monomer **10**, reflecting a much longer effective conjugation length over the extended coplanarized dithienosilole polymer backbone. However, it was noted that the film of polymer **12** showed the maximum absorbance wavelength at 498 nm; 4 nm blue-shifted compared with its solution counterpart (Figure 1a). The band gap of polymer **12** in the solid state is estimated to be 1.91 eV based on its film onset absorption wavelength. The observed blue-shift arises, most probably, from a less coplanar configuration associated with the more compact molecular arrangements in the solid state.

In contrast to polymer **12**, polymer **13** exhibited a red-shifted and much more broadened absorption in the solid state with respect to its solution absorption in THF (Figure 1b). The optical band gap of polymer **13** in THF was estimated to be as low as 1.81 eV and was further reduced to 1.40 eV in the solid state. Similar changes in UV−vis spectra have been reported for rigid conjugated polymers with a strong interchain interaction and were taken as an indication for 2D $\pi-\pi$ stacking.[18,19]

The fluorescence emission spectra of **12** in THF at different concentrations at room temperature are given in Figure 2, which show broad emission bands with a bathochromic shift by increasing concentration. For instance, the broad emission band

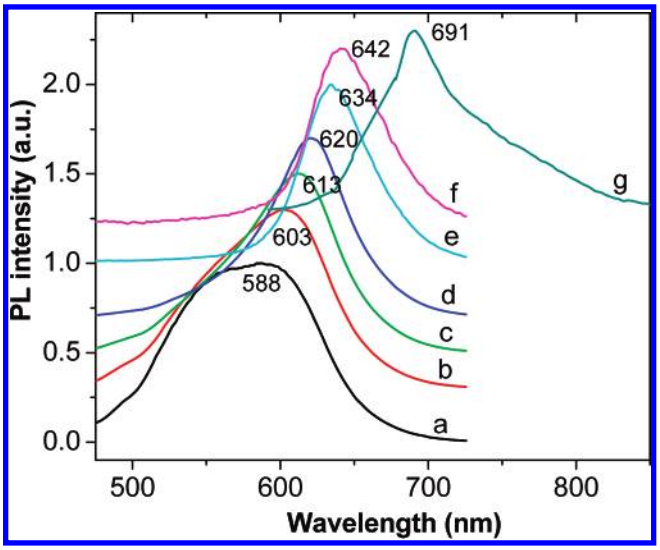

Figure 2. PL spectra of **12** solutions in THF at different concentrations. Key: (a) 2.5×10^{-7} M; (b) 5×10^{-7} M; (c) 1×10^{-6} M; (d) 5×10^{-6} M; (e) 1×10^{-5} M; (f) 1×10^{-4} M; (g) a solid-state film. The λ_{em}^{max} shifts from 588 to 691 nm with the concentration changes. The spectra were offset for clarity (excitation wavelength: 515 nm for solutions and 540 nm for the film).

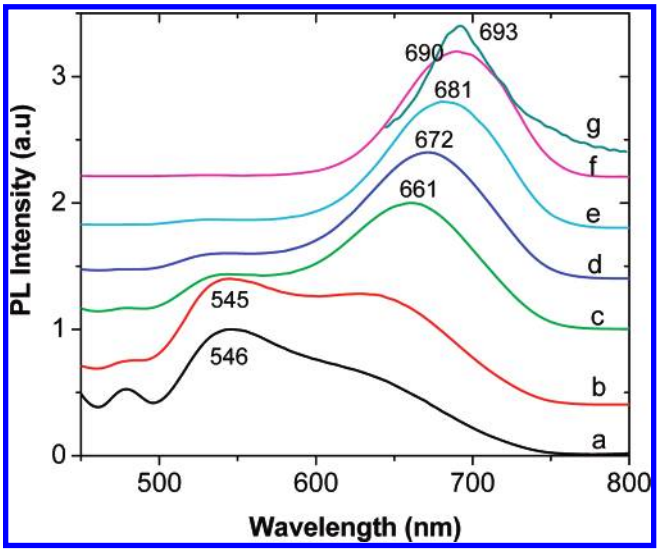

Figure 3. PL spectra of **13** solutions in THF at different concentrations. Key: (a) 2.5×10^{-7} M; (b) 5×10^{-7} M; (c) 1×10^{-6} M; (d) 5×10^{-6} M; (e) 1×10^{-5} M; (f) 1×10^{-4} M; (g) a solid-state film. The spectra were offset for clarity (excitation wavelength: 521 nm for solutions and 590 nm for the film).

over 500−670 nm peaked at about 588 nm (λ_{em}^{max}) for the THF solution of **12** at 2.5×10^{-7} M was found to red-shift up to 642 nm for the same solution with a concentration of 1.0×10^{-4} M. The shoulder peak at ~565 nm in the fluorescence spectra of those diluted **12** solutions (curves a and b in Figure 2) may come from the oligomers with relatively shorter conjugation lengths. With the increase in the polymer concentration and thus the formation of *J*-aggregate, the emission red-shifted to longer wavelengths, leading to overlapping with the peak at higher wavelengths. The corresponding PL emission spectrum from a polymer **12** film showed a relatively weak broad peak centered at *ca.* 691 nm (Figure 2g). Similar changes in the fluorescence emission were observed for **13**, as shown in Figure 3. The observed concentration-dependent red-shift in the fluorescence emissions for both **12** and **13** is presumably because these polymer chains take a more planar conformation in an aggregated state at high concentrations, as is the cases for

Table 1. Physical Properties of Polymers 12 and 13

polymer	T_g (°C)	λ_{max} (nm)[a]	λ_{max} (nm)[b]	E_{HOMO}[c] (eV)	E_{LUMO}[c] (eV)
12	83	502	498	4.85	N.A.[d]
13	114	563	593	5.13	3.23

[a] In THF solution. [b] In the solid state. [c] Estimated from the onset potentials using empirical equations: $E_{HOMO} = E'_p + 4.38$ eV and $E_{LUMO} = E'_n + 4.38$ eV. [d] No cathodic reduction wave was observed.

other silole-containing (macro)molecules.[26] The PL quantum efficiencies of **12** and **13** in THF solutions were determined with fluorescein as a reference[27] to be 1.1% and 0.6%, respectively. The corresponding values for solid films should be even lower, as is the case for many other conjugated polymers. The relatively low PL quantum efficiencies of **12** and **13**, together with the broad and strong optical absorption, suggested their potential for photovoltaic applications described below.

Electrochemical Study. To investigate the electrochemical properties of polymers **12** and **13** and estimate their HOMO and LUMO energy levels, cyclic voltammetry (CV) was carried out using a Pt disk (1 mm diameter), a Pt wire (0.5 mm diameter), and a silver wire (2 mm diameter) as the working electrode, counter electrode, and quasi-reference electrode, respectively. CV measurements were conducted in a 0.1 M Bu_4NPF_6 acetonitrile solution under Ar at a scan rate of 50 mV s^{-1}. Polymers **12** and **13** were coated on the working electrode. Prior to the CV study, the Ag quasi-reference electrode was first calibrated using a ferrocene/ferrocenium (Fc/Fc^+) redox couple (0.35 V vs Ag/AgCl)[28] as an external standard, and was found to be −0.02 V vs SCE. Therefore, the LUMO and HOMO energy levels of polymers **12** and **13** can be estimated using the empirical equations, $E_{HOMO} = E'_p + 4.38$ eV and $E_{LUMO} = E'_n + 4.38$ eV, respectively, where E'_p and E'_n are the onset potentials for oxidation and reduction relative to the Ag quasi-reference electrode, respectively. The results are summarized in Table 1, along with some other physical properties.

Figure 4 displays the CV curves for polymers **12** and **13**. Both the anodic oxidation and cathodic reduction processes of **13** are reversible. This ambipolar properties can be attributed to the unique structure of polymer **13**, which consists of alternating hole transporting dithienosilole (DST) moieties and electron-deficient 2,1,3-benzothiadiazole units. On the contrary, no cathodic reduction peak could be detected for polymer **12**, implying the difficulty in injecting electrons into this material. It is worth pointing out that the HOMO energy level of polymer **13** was lowered by 0.28 eV *via* the incorporation of electron withdrawing units into the polymer backbone, as compared with polymer **12**. The HOMO and LUMO levels of polymer **13** were estimated to lie at 5.13 and 3.23 eV, respectively. The electrochemical energy gap (1.9 eV for polymer **13** films) is higher than the optically measured one, probably due to the interfacial energy barrier for charge injection.[29]

Photovoltaic Properties. In order to investigate the potential use of polymers **12** and **13** in organic solar cells, bulk-heterojunction PV devices were fabricated in which the polymer was blended in a 1:1 weight ratio with the complementary fullerene-based electron acceptor, PCBM. Devices with the structure ITO/PEDOT−PSS/polymer **12** or **13**:PCBM(1:1)/Al were fabricated by first depositing a thin layer (∼35 nm) of PEDOT−PSS onto patterned ITO slides. The active layer was then deposited on the PEDOT:PSS film, and deposition of an aluminum back electrode completed the device structure (see Experimental Section for details).

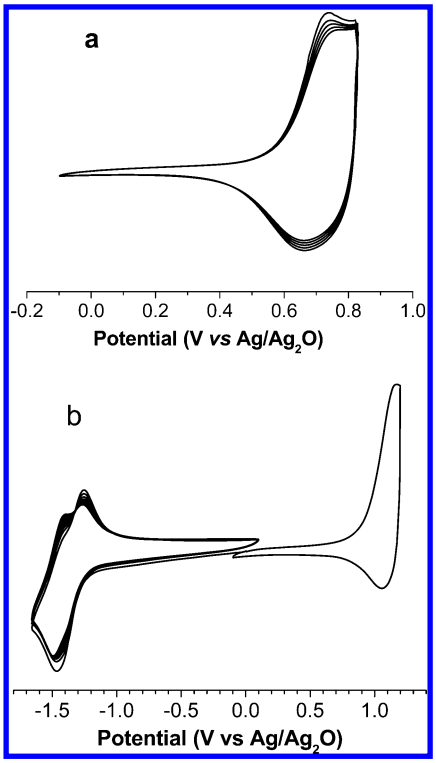

Figure 4. CV curves of polymer **12** (a) and **13** (b) films with 0.1 M Bu_4NPF_6 in acetonitrile as the supporting electrolyte.

For both polymer **12** and **13** based devices, the optimum active layer thickness was found in the range of 70 to 90 nm. Devices that were considerably thicker exhibited larger absorption cross sections, but with significantly lower short-circuit currents due to high series resistance. On the other hand, devices with thinner active layers (<50 nm) maintained a relatively high I_{sc}. However, the very low voltages (<0.01) reduced the achievable power output, due most probably to the presence of pinholes.

Annealing Effects. It has recently been shown that P3HT:PCBM-based bulk-heterojunction devices exhibit an enhancement in power conversion efficiency by approximately a factor of 5 after annealing at 120−150 °C.[25,30] This increase in performance has been attributed to improved charge mobility brought about by the formation of ordered nanostructures. To determine if a similar enhancement could be thermally induced for polymers **12** and **13** based devices, current−voltage measurements were taken while heating through periodic (10 °C) temperature increases in situ. The comparison of PV performance before and after the thermal treatment is shown in Figure 5. The enhanced device performance is likely due to a possible thermal-induced reorganization of active components and subsequent improvements in charge mobility. However, it should be noted that the degree of improvement for devices comprised polymers **12** and **13** is much smaller than that observed for P3HT devices. This is not surprising given the amorphous nature of both polymers **12** and **13**. In contrast, P3HT is a highly crystalline material, which shows a pronounced red-shift in UV−vis spectra after thermal treatment.

The difference in the PV performance between polymer **12** and **13** may lie in the nature of the polymer backbone. The presence of internal electron donor−acceptor charge-transfer interaction and strong interchain interaction in polymer **13** resulted in extended absorption in the solar spectrum, and thus a better power conversion efficiency. Table 2 summarizes the PV performance for the polymer **12** and **13** based devices under AM 1.5 simulated solar illumination.

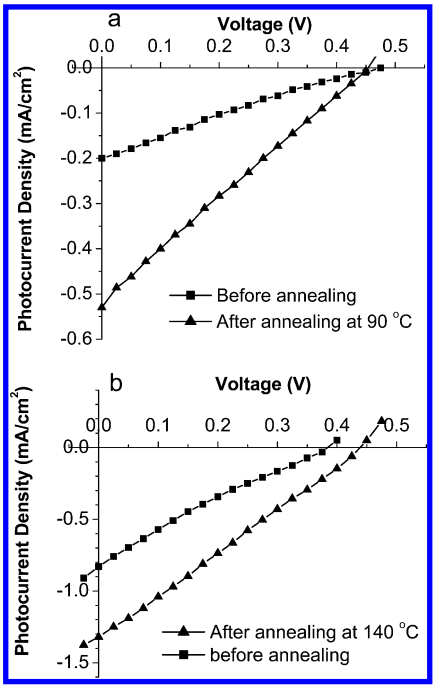

Figure 5. I−V characteristics of polymer (a) **12** and (b) **13** based devices under AM 1.5 simulated solar illumination at an intensity of 100 mW/cm^2.

Table 2. Typical Photovoltaic Performance of Polymers 12 and 13 Based Solar Cells under Simulated AM 1.5 Solar Illumination (100 mW/cm^2)

polymer	V_{oc} (V)	J_{sc} (mA/cm^2)	*FF*	PCE (%)
12	0.47[a]	0.20[a]	0.21[a]	0.02[a]
	0.45[b]	0.52[b]	0.22[b]	0.051[b]
13	0.38[a]	0.83[a]	0.22[a]	0.07[a]
	0.44[b]	1.32[b]	0.31[b]	0.18[b]

[a] For as-fabricated devices. [b] For annealed devices.

The evolution of the power conversion efficiency with operating temperatures is shown in Figure 6. As can be seen from Figure 6, the optimum operating temperature for polymers **12** and **13** based devices was 90 and 140 °C, respectively. Polymer **13** exhibited the most significant improvement in maximum power output/efficiency (a factor of 3) upon annealing. Specifically, the device parameters improved from I_{sc} = 0.83 mA/cm^2, V_{oc} = 0.38 V, and PCE = 0.07% at room temperature to I_{sc} = 1.32 mA/cm^2, V_{oc} = 0.44 V, and PCE = 0.18% at 140 °C. The improvement in efficiency with increasing temperature could be due to the formation of phase-separated structures and increased charge mobilities at higher temperatures. However, overheating the devices above the optimum operating temperature resulted in irreversible damage to the device. This could be ascribed to the over-growth of the PCBM phase and/or the occurrence of interface delamination at temperatures well above the T_g of the polymer matrix.[31]

External Quantum Efficiency. Figure 7 displays the external quantum efficiency (EQE) spectra for the devices using the polymer **12** or **13**:PCBM (1:1) blend as the photoactive layer. Polymer **12** based devices exhibit PV response peaks at 340 and 425 nm, as well as a shoulder at 550 nm, which coincide largely with those in the absorption spectra of the individual components. The absorption spectrum (not shown) of the polymer 12:PCBM blend is a simple linear superposition of the component absorption spectra, suggesting that there is no ground state interaction between the two components. However, the origin of the additional peak at 425 nm in the EQE spectrum is not clear at this moment. Interestingly, the current response over

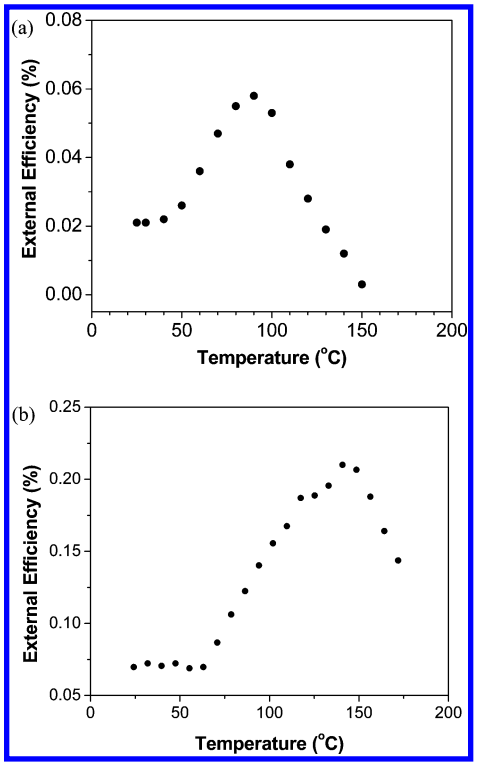

Figure 6. Power conversion efficiency as a function of operating temperatures for polymer (a) **12** and (b) **13** based devices.

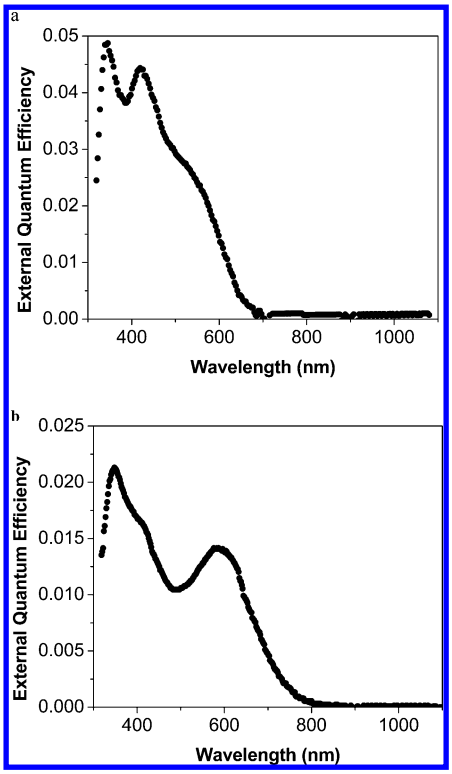

Figure 7. EQE spectra for the PV devices using the polymer (a) **12** or (b) **13**:PCBM (1:1) blend as the photoactive layer.

the polymer absorption regions contributed at a less extent than expected to the overall device response. The EQE spectrum for a **13**:PCBM blend based device is shown in Figure 7b. There are two peaks at 350 and 580 nm, and a shoulder at 400 nm. In contrast to polymer **12**, the measured current in the region of the polymer absorption comprises a large portion of that obtained over the tested range, suggesting that this polymer is somehow contributing significantly to the overall current generated by

the **13**:PCBM based device under illumination presumably due to the effective intramolecular charge transfer.

Conclusions

Dithienosilole-containing homopolymer **12** and alternating copolymer **13** (Scheme 2) were synthesized and their optical absorption, fluorescence, and photovoltaic properties were investigated. Polymers **12** and **13** in THF solution demonstrated absorption peaks at 502 and 563 nm, respectively; polymer **13** displayed pronounced red-shifts upon the formation of the corresponding solid films due to the presence of electron-withdrawing benzothiadiazole moieties along the dithienosilole units that effectively extend the conjugation length along the polymer backbones through 2D $\pi-\pi$ stacking. Bulk-heterojunction organic solar cells were fabricated with configuration of ITO/PEDOT:PSS/**12** or **13**:PCBM (1:1)/Al and examined under AM 1.5 simulated solar illumination. The best PV performance was obtained from the polymer **13** based devices after thermal annealing at 140 °C with an open-circuit voltage of 0.44 V, a short-circuit current density of 1.32 mA/cm^2, and an overall power conversion efficiency of 0.18%. Given the low values of the fill-factor listed in Table 2, it is likely that the photovoltaic performance can be further improved by optimizing the polymerization conditions to improve polymer purity and crystallinity, the ratio of the polymer to PCBM, and/or device fabrication conditions. Therefore, this study does provide new concepts for enhancing light harvesting (via the synthesis of silole-containing low-band gap conjugated polymers with strong internal electron donor−acceptor interactions) and for improving the device performance through the morphology control of the silole-containing conjugated polymer photovoltaic layers by thermal annealing, though the value of the power conversion efficiency obtained so far for these unoptimized solar cells is still relatively low.

Acknowledgment. Financial support of this work from AFOSR (FA9550-06-1-0384) and AFRL/ML-HBCU is gratefully acknowledged.

References and Notes

(1) Luo, J.; Xie, Z.; Lam, J. W. Y.; Cheng, L.; Chen, H.; Qiu, C.; Kwok, H. S.; Zhan, X.; Liu, Y.; Zhu, D.; Tang, B. Z. *Chem. Commun.* **2001**, 1740−1741.
(2) Chen, H. Y.; Lam, J. W. Y.; Luo, J. D.; Ho, Y. L.; Tang, B. Z.; Zhu, D.; Wong, M.; Kwok, H. S. *Appl. Phys. Lett.* **2002**, *81*, 574−576.
(3) Chen, J.; Xie, Z.; Lam, J. W. Y.; Law, C. C. W.; Tang, B. Z. *Macromolecules* **2003**, *36*, 1108−1117.
(4) Yamaguchi, S.; Tamao, K. Polysiloles and related siole-containing polymers. In *The Chemistry of Organic Silicon Compounds*; Rappoport, Z., Apeloig, Y., Eds. John Wiley & Sons, Ltd.: Chichester, U.K., 2001; pp 641−694.
(5) Yamaguchi, S.; Endo, T.; Uchida, M.; Izumizawa, T.; Furukawa, K.; Tamao, K. *Chem. Eur. J.* **2000**, *6*, 1683−1692.
(6) Kunai, A.; Ohshita, J.; Iida, T.; Kanehara, K.; Adachi, A.; Okita, K. *Synth. Met.* **2003**, *137*, 1007−1008.
(7) Ohshita, J.; Nodono, M.; Kai, H.; Watanabe, T.; Kunai, A.; Komaguchi, K.; Shitotani, M.; Adachi, A.; Okita, K.; Harima, Y.; Yamashita, K.; Ishikawa, M. *Organometallics* **1999**, *18*, 1453−1459.
(8) Tamao, K.; Uchida, M.; Izumizawa, T.; Furukawa, K.; Yamaguchi, S. *J. Am. Chem. Soc.* **1996**, *118*, 11974−11975.
(9) Ohshita, J.; Kai, H.; Takata, A.; Iida, T.; Kunai, A.; Ohta, N.; Komaguchi, K.; Shiotani, M.; Adachi, A.; Sakamaki, K.; Okita, K. *Organometallics* **2001**, *20*, 4800−4805.
(10) Usta, H.; Lu, G.; Facchetti, A.; Marks, T. J. *J. Am. Chem. Soc.* **2006**, *128*, 9034−9035.
(11) Kim, D. H.; Ohshita, J.; Lee, K.-H.; Kunugi, Y.; Kunai, A. *Organometallics* **2006**, *25*, 1511−1516.
(12) Scharber, M. C.; Muhlbacher, D.; Koppe, M.; Denk, P.; Waldauf, C.; Heeger, A. J.; Brabec, C. J. *Adv. Mater.* **2006**, *18*, 789.
(13) Ohshita, J.; Sumida, T.; Kunai, A.; Adachi, A.; Sakamaki, K.; Okita, K. *Macromolecules* **2000**, *33*, 8890−8893.
(14) Ohshita, J.; Kai, H.; Sumida, T.; Kunai, A.; Adachi, A.; Sakamaki, K.; Okita, K. *J. Organomet. Chem.* **2002**, *642*, 137−142.
(15) Wong, W. Y.; Wang, X. Z.; He, Z.; Djurišić, A. B.; Yip, C. T.; Cheung, K. Y.; Wang, H.; Mak, C. S.; Chan, W. K. *Nat. Mater.* Published online 13 May 2007.
(16) (a) Roquet, S.; Cravino, A.; Leriche, P.; Alévêque, O.; Frère, P.; Roncali, J. *J. Am. Chem. Soc.* **2006**, *128*, 3459−3466. (b) Zhang, C.; Choi, S.; Haliburton, J.; Cleveland, T.; Li, R.; Sun, S. S.; Ledbetter, A.; Bonner, C. E. *Macromolecules* **2006**, *39*, 4317.
(17) Mühlbacher, D.; Scharber, M.; Morana, M.; Zhu, Z.; Waller, D.; Gaudiana, R.; Brabec, C. *Adv. Mater.* **2006**, *18*, 2884.
(18) Schulze, K.; Uhrich, C.; Schüooel, R.; Leo, K.; Pfeiffer, M.; Brier, E.; Reinold, E.; Bäuerle, P. *Adv. Mater.* **2006**, *18*, 2872.
(19) Brown, P. J.; Thomas, D. S.; Köhler, A.; Wilson, J. S.; Kim, J. S.; Ramsdale, C. M.; Sirringhaus, H.; Friend, R. H. *Phys. Rev. B: Condens. Mater. Mater. Phys.* **2003**, *67*, 642031.
(20) Edelmann, M. J.; Raimundo, J.-M.; Utesch, N. F.; Diederich, F.; Boudon, C.; Gisselbrecht, J.-P.; Gross, M. *Helv. Chim. Acta* **2002**, *85*, 2195−2213.
(21) Li, Z. H.; Wong, M. S.; Fukutani, H.; Tao, Y. *Chem. Mater.* **2005**, *17*, 5032.
(22) Lee, K. H.; Ohshita, J.; Kimura, K.; Kunugi, Y.; Kunai, A. *J. Organomet. Chem.* **2005**, *690*, 333−337.
(23) Blouin, N.; Michaud, A.; Leclerc, M. *Adv. Mater.* **2007**, *19*, 2295.
(24) Lu, J.; Xia, P.; Lo, Tao, P.; Y.; Wong, M. *Chem. Mater.* **2006**, *18*, 6194.
(25) Ma, W.; Yang, C.; Gong, X.; Lee, K.; Heeger, A. J. *Adv. Funct. Mater.* **2005**, *15*, 1617.
(26) (a) Wang, F.; Luo, J.; Yang, K.; Chen, J.; Huang, F.; Cao, Y. *Macromolecules* **2005**, *38*, 2253−2260. (b) Chen, J. W.; Kwok, H. S.; Tang, B. Z. *J. Polym. Sci., Part A* **2006**, *44*, 2487.
(27) Geng, Y.; Chen, A. C. A.; Ou, J. J.; Chen, S. H. *Chem. Mater.* **2003**, *15*, 4352−4360.
(28) (a) de Leeuw, D. M.; Simenon, M. M. J.; Brown, A. R.; Einerhand, R. E. F. *Synth. Met.* **1997**, *87*, 53. (b) Cui, Y.; Zhang, X.; Jenekhe, S. A. *Macromolecules* **1999**, *32*, 3824.
(29) Chen, Z. K.; Huang, W.; Wang, L. H.; Kang, E. T.; Chen, B. J.; Lee, C. S.; Lee, S. T. *Macromolecules* **2000**, *33*, 9015.
(30) Kim, Y.; Choulis, S. A.; Nelson, J.; Bradley, D. D. C.; Cook, S.; Durrant, J. R. *Appl. Phys. Lett.* **2005**, *86*, 63502.
(31) Yang, X.; van Duren, J. K. J.; Janssen, R. A. J.; Michels, M. A. J.; Loos, J. *Macromolecules* **2004**, *37*, 2151−2158.

MA071825X